Fibers and Polymers (2026) 27:435–451
https://doi.org/10.1007/s12221-025-01218-2

Online ISSN 1875-0052
Print ISSN 1229-9197

REGULAR ARTICLE

Deep Learning-Based Fiber Orientation Analysis for Discontinuous Composites: Application to Material Extrusion Additive Manufacturing

César García-Gascón[1,2] · Javier Bas-Bolufer[1] · Pablo Castelló-Pedrero[1,2] · Francisco Chinesta[2,3]

Received: 14 May 2025 / Revised: 20 August 2025 / Accepted: 11 October 2025 / Published online: 31 October 2025

Abstract
This paper presents a novel deep learning-based (DL) approach to characterize short-fiber orientation in material extrusion large format additive manufacturing (LFAM). The method focuses on Acrylonitrile Butadiene Styrene (ABS) reinforced with short glass fibers 20%, a material widely used due to its enhanced mechanical performance. Traditional fiber orientation analysis, which relies on microscopy and manual image processing, is often costly and time-consuming. To address this, we developed Python algorithms to generate synthetic SEM-like images to train a Convolutional Neural Network (CNN). The proposed CNN accurately predicts the fiber orientation tensors directly from micrographs, with consistent results with conventional methods. The combination of synthetic data generation and deep learning provides a scalable and rapid alternative for fiber orientation analysis. This approach improves the analysis of fiber orientation in discontinuous composite materials and has the potential to be applied to additive manufacturing and other forming processes. This study demonstrates that combining deep learning with synthetic data generation provides an effective, scalable solution for fiber orientation analysis in LFAM, confirming that CNN-based methods can greatly improve material characterization. More accurate performance prediction and quality control could be achieved in fiber-reinforced additive manufacturing.

Keywords Deep learning · Neural network · Fiber orientation · Additive manufacturing

1 Introduction

Large Format Additive Manufacturing (LFAM), also known as Material Extrusion Large Format Additive Manufacturing (MEX-LFAM), is an extrusion-based technology to fabricate large-scale components for industries, such as automotive, aerospace, and wind energy [1]. This work focuses on Acrylonitrile Butadiene Styrene (ABS) reinforced with 20% short Glass Fibers (GF). Convolutional Neural Networks (CNNs) trained on Scanning Electron Microscopy (SEM)-like images are leveraged to characterize fiber orientation tensors.

LFAM enables rapid production of composite parts and tooling, although finishing operations, such as milling or polishing, may be necessary to achieve precise dimensional and surface quality specifications [2]. This process aligns the fibers (approximately 0.6 mm in length) predominantly along the extrusion direction, orienting up to 95% of the fibers along this axis [3, 4]. This alignment doubles stiffness and significantly improves heat transfer in carbon fiber composites [5]. In addition, thermodynamic properties have a fundamental influence on determining the quality of parts [6]. This process can be used to process high-performance thermoplastics, such as polyetheretherketone (PEEK) and polyetherimide (PEI, commercially known as Ultem), which are renowned for their exceptional thermal, mechanical, and chemical properties. However, the structural performance of

✉ César García-Gascón
cegarga3@etsid.upv.es

Javier Bas-Bolufer
jababo@etsii.upv.es

Pablo Castelló-Pedrero
pabcaspe@idf.upv.es

Francisco Chinesta
francisco.chinesta@ensam.eu

1 Design and Manufacturing Research Institute, Universitat Politècnica de València, Camino de Vera, s/n, 46022 València, València, Spain

2 PIMM Laboratory, Arts et Métiers Institute of Technology, CNRS, ENSAM, boulevard de l'Hôpital, 151, 75013 Paris, France

3 CNRS@CREATE Ltd, Organization, 1 Create Way, #08-01 CREATE Tower, Singapore 138602, Singapore

these materials depends heavily on fiber orientation. Accurate fiber orientation characterization is therefore essential for reliable structural validation and certification, particularly in sectors, such as aerospace, automotive, and tooling, where LFAM is becoming increasingly popular. The proposed method's ability to efficiently and accurately assess fiber alignment directly contributes to these certification processes.

Numerical simulation methods and artificial intelligence approaches have significantly improved the understanding of fiber orientation in composite materials [3]. Advani and Tucker [7] developed a mathematical framework using tensor-based representations to model and predict fiber orientation in short fiber-reinforced composites. This method enables the computation of orientation distributions from fiber evolution, which becomes essential for computational modeling in injection molding and composite design. Orientation tensors provided a compact and comprehensive representation of fiber orientation, which allowed easyon of fiber orientation models into both computational fluid dynamics (CFD) and finite element analysis (FEA) systems [8].

Tucker III [9] presented several advances in fiber characterization, highlighting experimental and computational techniques specifically developed to quantify and predict the fiber orientation distribution in composite materials. The review analyzed basic mathematical tools such as probability distribution functions together with higher-order orientation tensors, which have become standard components of numerical simulations for fiber-reinforced composites. Bleiziffer et al. [3] proposed a CNN-based approach to predict fiber orientation in composite materials using micro-computed tomography (μ-CT) images, demonstrating that DL can significantly enhance fiber orientation analysis compared to traditional moment of inertia methods. However, their approach was limited to supervised learning on experimental datasets. In contrast, Li et al. [10] introduced a more comprehensive DL framework that incorporates real-time corrections through a collaborative optimization mechanism. Their methodology improved fiber orientation predictions by dynamically refining the CNN model using elite training samples, leading to better adaptability and generalization in composite manufacturing applications.

Herrmann et al. [11] study the use of neural networks to predict fiber orientation tensors in injection-molded short fiber-reinforced plastics, drastically reducing the computational effort compared to classical simulation methods. The study evaluated various DL architectures, demonstrating that Long Short-Term Memory networks (LSTMs) achieved the highest prediction accuracy, whereas CNNs and Deep Neural Networks (DNNs) offered superior computational efficiency [12]. Neural networks significantly reduce prediction time, approximately one ten-thousandth of the original duration, making them ideal for rapid design iterations. However, their accuracy strongly depends on the quality of training data, necessitating integration with high-quality experimental or simulation-based datasets.

The deposition path during material extrusion additive manufacturing processes directly determines fiber orientation. Šeta et al. [8] developed a three-dimensional computational model to simulate fiber orientation alongside strand morphology within material extrusion additive manufacturing (MEX-LFAM). The model used computational fluid dynamics (CFD) together with fiber interaction mechanics to study the effects of extrusion speed, flow rate, and die geometry as well as rheological properties on fiber orientation. By adjusting process parameters, the researchers were able to control fiber orientation, resulting in anisotropic composites with tailored mechanical properties. Li et al. [13] introduced an effective topology optimization method through DL for continuous fiber-reinforced composite structures in 2025. The method used a ResUNet-based Generative Adversarial Network (GAM) to create an optimal fiber layout, while at the same time achieving improved design efficiency and structural performance. An Independent Continuous Mapping (ICM) method enabled the development of topology optimization datasets with accurate representations of fiber angles within composite structures. The study demonstrated how generative artificial intelligence methodologies could refine structural engineering designs and facilitate the automatic development of composite structures. Kalimullah et al. [6] introduced a probabilistic machine learning framework which allows for the measurement of stiffness tensors in carbon composite laminates.

Future research efforts are expected to focus on developing hybrid frameworks that combine physics-informed machine learning (PIML) and artificial intelligence (AI). Such integration aims to improve model generalization and interpretability by explicitly incorporating governing physical equations [14]. Hybrid methods enhance purely data-driven models by directly embedding physical constraints into neural network architectures. Advances in high-resolution imaging techniques, such as X-ray microtomography combined with AI-assisted image segmentation, promise significant improvements in the accuracy of fiber orientation measurements. While deep learning methods achieve high predictive accuracy, their reliance on extensive annotated datasets limits broader applicability. Generative models, including VAEs and GANs, can generate realistic synthetic datasets, thereby alleviating data scarcity issues commonly encountered in machine learning-based fiber orientation analysis.

This work presents a deep learning-based methodology for characterizing fiber orientation in composites produced via MEX-LFAM. The approach uses synthetic datasets generated by Python-based algorithms to simulate SEM images with controlled fiber orientation distributions. These images were used to train a CNN capable of predicting the components of the orientation tensor directly from binarized images (binary micrographs). While the proposed methodology can be applied to various composite manufacturing processes, LFAM is a particularly demanding use case due to the anisotropic behavior, large part size, and high thermal gradients. These factors make accurate and scalable fiber orientation analysis especially critical.

To provide a comprehensive understanding of the proposed methodology, this paper is structured as follows: Sect. 2 describes the materials used and the experimental workflow, including sample preparation, image acquisition, and fiber orientation analysis using microscopy. It also introduces the synthetic data generation process and the CNN architecture used in this study. Section 3 presents and discusses the results obtained from the CNN training and validation, highlighting the performance and accuracy of the model for different metrics. Finally, Sect. 4 outlines the main conclusions of the work and proposes future directions to improve fiber orientation characterization through the integration of physics-based learning and advanced imaging techniques. The list of abbreviations and acronyms used in the article are listed in Table 1.

This study makes three main contributions: (i) a physically motivated generator of synthetic SEM-like images with known orientation tensors, enabling the creation of large annotated datasets; (ii) a compact CNN architecture that directly regresses fiber orientation tensors from micrographs, validated with cross-validation ($R^2 \approx 0.989$); and (iii) a fully specified, reproducible workflow for preprocessing and analysis, ensuring transparency and replicability.

Table 1 List acronyms

Acronym	Meaning
ABS	Acrylonitrile Butadiene Styrene
AI	Artificial Intelligence
CFD	Computational Fluid Dynamics
CNN	Convolutional Neural Network
DL	Deep Learning
DNN	Deep Neural Networks
FEA	Finite Element Analysis
GAN	Generative Adversarial Network
GF	Glass Fiber
ICM	Independent Continuous Mapping
JSD	Jensen–Shannon Divergence
LFAM	Large Format Additive Manufacturing
LSTM	Long Short-Term Memory networks
MAE	Mean Absolute Error
MAPE	Mean Absolute Percentage Error
MEX-LFAM	Material Extrusion Large Format Additive Manufacturing
MLP	Multi-Layer Perceptron
MSE	Mean Squared Error
PIML	Physics-Informed Machine Learning
PINN	Physics-Informed Neural Network
ReLU	Rectified Linear Unit
RMSE	Root Mean Squared Error
R^2	Coefficient of Determination
SEM	Scanning Electron Microscopy
VAE	Variational Autoencoder

2 Materials and Methods

2.1 Materials and LFAM Process

In this study, LFAM technology was employed to fabricate composite samples composed of Acrylonitrile Butadiene Styrene (ABS) reinforced with 20% short glass fibers (GF). The printed structures were analyzed using various microscopy techniques to characterize fiber orientation and quantify the anisotropic properties of the composite material. To support neural network training and validation, a synthetic image generation routine was developed in Python, producing a robust dataset of 40,000 images that accurately simulated fiber microstructural distributions under controlled conditions. A machine learning model was subsequently trained exclusively on these synthetic datasets to predict the orientation tensor directly from microscopy images.

Figure 1 presents polished cross-section images of an LFAM composite part containing 20% glass fibers, observed from two perpendicular perspectives. The (a) image shows a 3D reconstruction that illustrates fiber alignment parallel to the flow direction during material deposition. The three central images display cross-sections along distinct planes, revealing variations in fiber orientation. Although the 3D view provides information about fiber density and volume fraction, it does not explicitly show orientation. Therefore, cross-sectional slices obtained perpendicular and parallel to the extrusion direction, as shown in the central images, are essential for accurate analysis of fiber alignment. The three central images display cross-sections along distinct planes, revealing variations in fiber orientation. Although the 3D view provides information about fiber density and volume fraction, it does not explicitly show orientation. Therefore, cross-sectional slices obtained perpendicular and parallel to the extrusion direction, as shown in the central images, are essential for accurate analysis of fiber alignment. The elongated elliptical shapes of the fibers in these sections indicate their alignment with the extrusion path, as observed in a cross-sectional slice taken perpendicular to the extrusion direction. By analyzing the degree of elongation, the aspect ratio and orientation relative to the printing direction can be determined. The (b) image illustrates the principal axes and

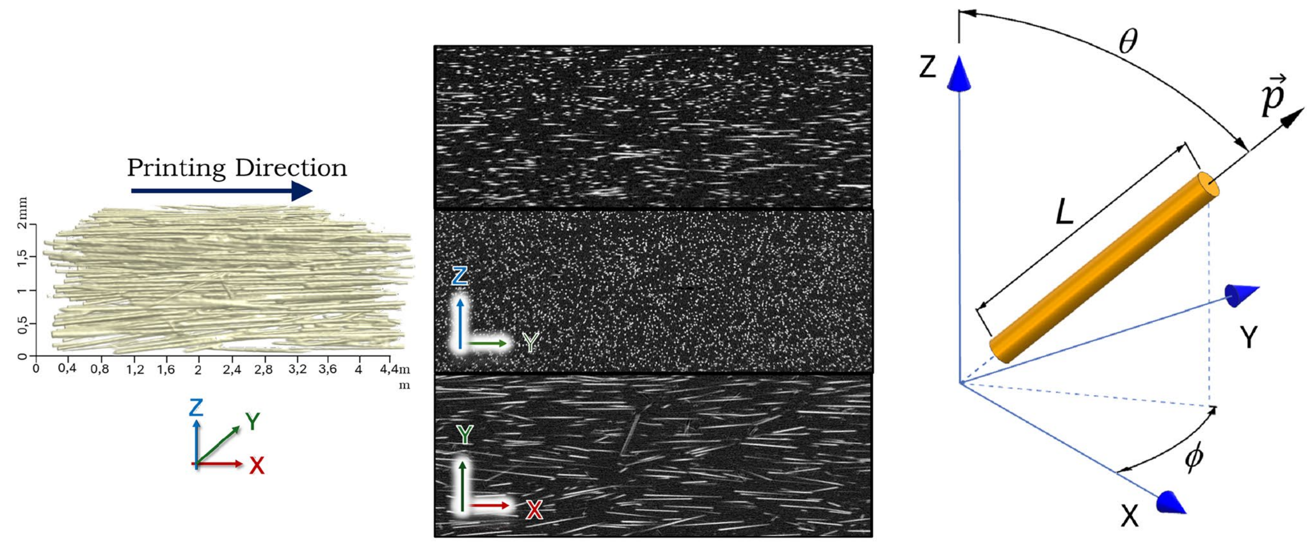

(a) Fiber orientation at different cutting planes. (b) Fiber angles [9].

Fig. 1 Polished cross-sections from an LFAM part containing 20% short GF. **a** 3D reconstruction and orthogonal planes (*xy*, *yz*, *xz*) with the extrusion/flow direction indicated; elongated ellipses denote fibers aligned with the bead path. **b** Principal material axes (*x*, *y*, *z*) and orientation angles used in tensor computation

the angular parameters used for the characterization of the fiber orientation.

In Fig. 1b, the axis z is defined as the surface normal, while the vector p represents the fiber direction. By definition, z is perpendicular to the sample plane, but the fiber direction p may not coincide with the in-plane axes and can present a tilt angle θ relative to z. This explains why p does not appear strictly perpendicular to z in the schematic.

It can be observed in Fig. 1a that the fiber orientation in the upper part of the zx-plane differs from the yx-plane. This discrepancy arises from the transition region between adjacent deposition layers, where the flow direction changes and local reorientation of the fibers occurs.

Figure 2 illustrates the impact of sectioning on the visualization of fiber orientation in composite materials. On the (a) image, a three-dimensional composite block with short fibers randomly dispersed within a polymer matrix is shown; the adjacent view isolates the fiber phase to emphasize its random three-dimensional distribution. On the right, the figure depicts the intersection of two parallel cutting planes with the composite block. Fibers oriented perpendicularly to the cutting plane manifest as circular cross-sections, while those aligned parallel to the plane yield elongated elliptical shapes (Figs. 2 and 3). Intermediate orientations result in ellipses of varying elongation, clearly revealing the anisotropic nature of fiber alignment in two-dimensional microscopy images. When cylindrical fibers intersect the cutting surface, their elliptical profiles—characterized by a major diameter (M) and a minor diameter (m)—facilitate the determination of spatial fiber orientation through trigonometric relationships

$$\cos\theta = \frac{m}{M}, \tag{1}$$

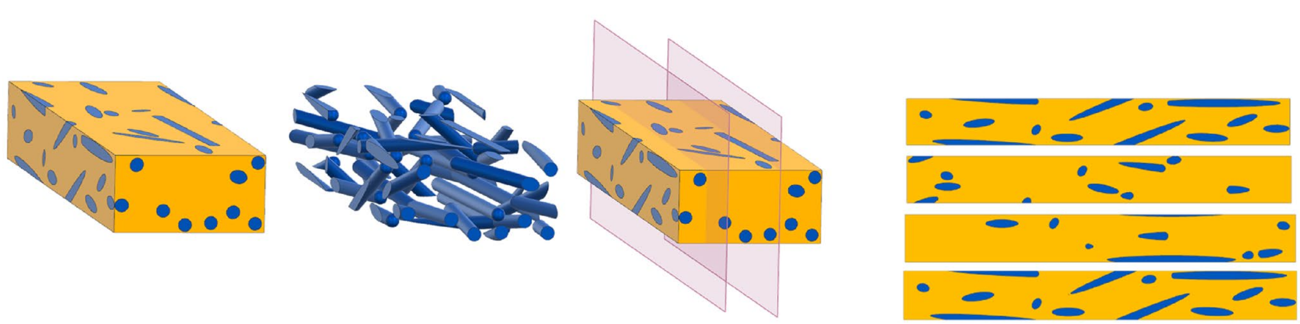

Fig. 2 Elementary representative volume and planar sections

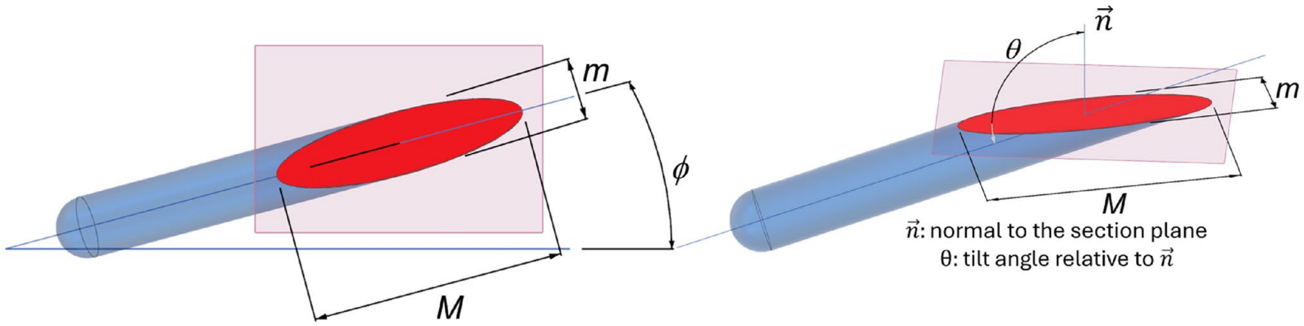

Fig. 3 Schematic of fiber-section intersection. A cylindrical fiber intersecting the cutting plane generates an elliptical profile characterized by major axis M and minor axis m. The normal to the plane (n) is explicitly indicated, and the tilt angle θ is defined relative to n. This figure illustrates the geometric basis for calculating the out-of-plane fiber tilt

where θ is the angle between the fiber axis and the normal to the section (Fig. 3). The orientation tensor is calculated by averaging the individual fiber contributions [9]

$$A_{ij} = \frac{\sum_{k=1}^{N} (p_i p_j)_k F_k}{\sum_{k=1}^{N} F_k}, \tag{2}$$

where p_i and p_j are the components of the unit vector describing the k-fiber orientation, and F_k is a weighting factor that corrects for bias due to the higher probability of intersection of fibers orientated perpendicular to the shear plane [9].

Despite its extensive utilization, this method is limited in a number of ways that affect the accuracy of fiber orientation measurements. Even minor inaccuracies during the measurement process can significantly affect results, especially in scenarios where fibers are oriented almost parallel to the sectioning plane, leading to large deviations in the computed orientations (Fig. 2). Consequently, the employment of high-resolution imaging in conjunction with advanced segmentation techniques is imperative to ensure the attainment of reliable and precise results. Additionally, the accuracy of fiber cross-section identification is contingent on the quality of the captured images.

To accurately determine the complete orientation tensor from two-dimensional images, it is necessary to adopt multiple complementary strategies to compensate for the loss of information inherent in representing three-dimensional fiber distributions in two-dimensional projections [9, 15]. A precise determination of each orientation tensor component can be obtained by analyzing three orthogonal cross-sections taken from the same specimen or an equivalent one, thereby effectively eliminating measurement uncertainties. Furthermore, the statistical correction method outlined in [9] addresses and mitigates biases introduced during the process of sample sectioning. Utilizing trigonometric relationships derived from two-dimensional projections, this method establishes upper and lower bounds for components of the orientation tensor that might otherwise remain ambiguous. Furthermore, the employment of advanced microscopy techniques facilitates a more detailed analysis of the samples without the necessity for additional physical sectioning. The combination of these approaches, which minimizes measurement uncertainties, significantly enhances the precision of fiber tilt angle determinations relative to the sectioning planes.

This research proposes an AI-driven methodology to significantly improve fiber orientation analysis. The proposed approach uses CNNs, which rely heavily on large image datasets for effective training. However, obtaining sufficient quantities of these images remains a challenge, especially since the model's performance depends directly on accurate image labeling—each image must be carefully annotated with its corresponding orientation tensor. To demonstrate the effectiveness of our method, we chose a composite material consisting of ABS reinforced with 20% short glass fibers (GF 20%). Figure 4 illustrates the MEX 3D printer used in this study. With a large build volume of $1500 \times 2500 \times 1000$ mm^3, this printer is particularly suitable for the production of large structural components essential in the aerospace, automotive, and tooling industries. In addition, the printer's extrusion head can operate at temperatures up to 400°C, enabling the use of advanced thermoplastic polymers, such as polyetheretherketone (PEEK) and polyetherimide (Ultem). These materials have exceptional thermal stability, mechanical strength, and chemical resistance [2].

To analyze the fiber orientation in the microstructure of the material, samples were prepared using the following steps. First, the analysis method started with cutting and encapsulation, then moved to image processing, followed by synthetic data generation for neural network training, and ended with the application of convolutional neural networks.

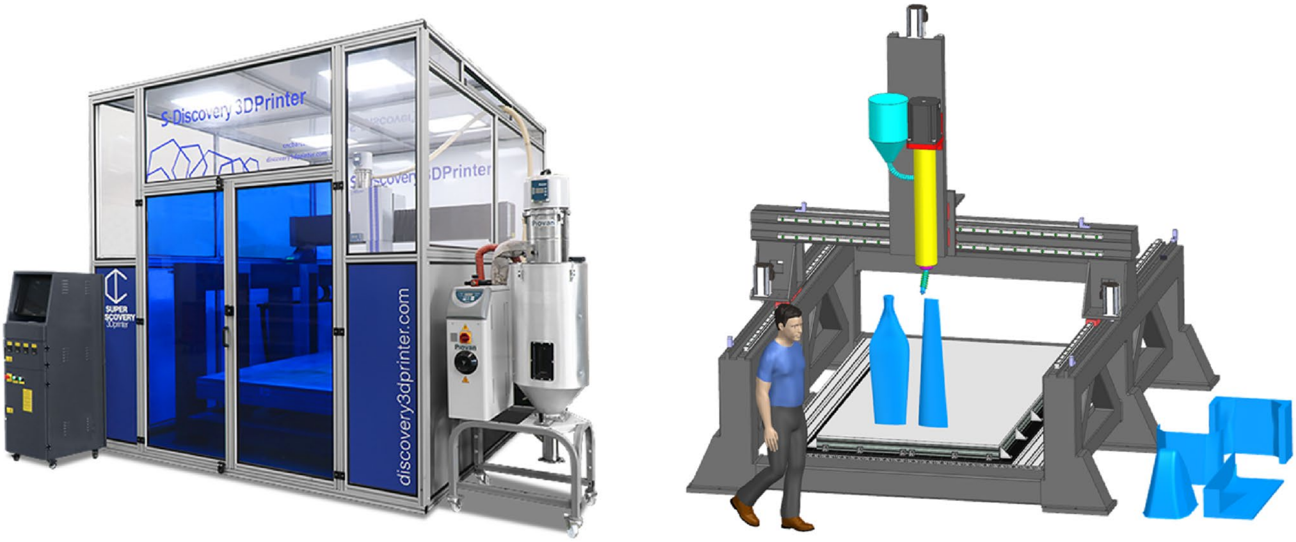

Fig. 4 Large format additive manufacturing printer

2.2 Sample Preparation and Encapsulation

A detailed sample preparation method was used to preserve the microstructure of the material while providing ideal conditions for analysis. The first step in sample preparation was cutting, followed by encapsulation in epoxy resin to provide structural support and facilitate handling during subsequent preparation and testing. The encapsulated specimens were mechanically ground and polished to produce a defect-free surface for microscopic analysis. Silicon carbide abrasive papers were used to process the samples, progressing from coarse grit for defect removal to finer grit to remove surface scratches and deformation layers. The use of 2000 grit paper revealed the fiber–matrix interface with great clarity during the process. The final polishing stage used diamond suspensions with progressively smaller particles until 1 μ m-diameter particles were achieved. Polishing the samples required a rotating disk held under controlled pressure to achieve a consistent surface finish on all samples.

High-resolution images of the fiber cross-sections (Fig. 5) were obtained by means of a Field Emission Scanning Electron Microscope (FESEM) of the prepared samples. The

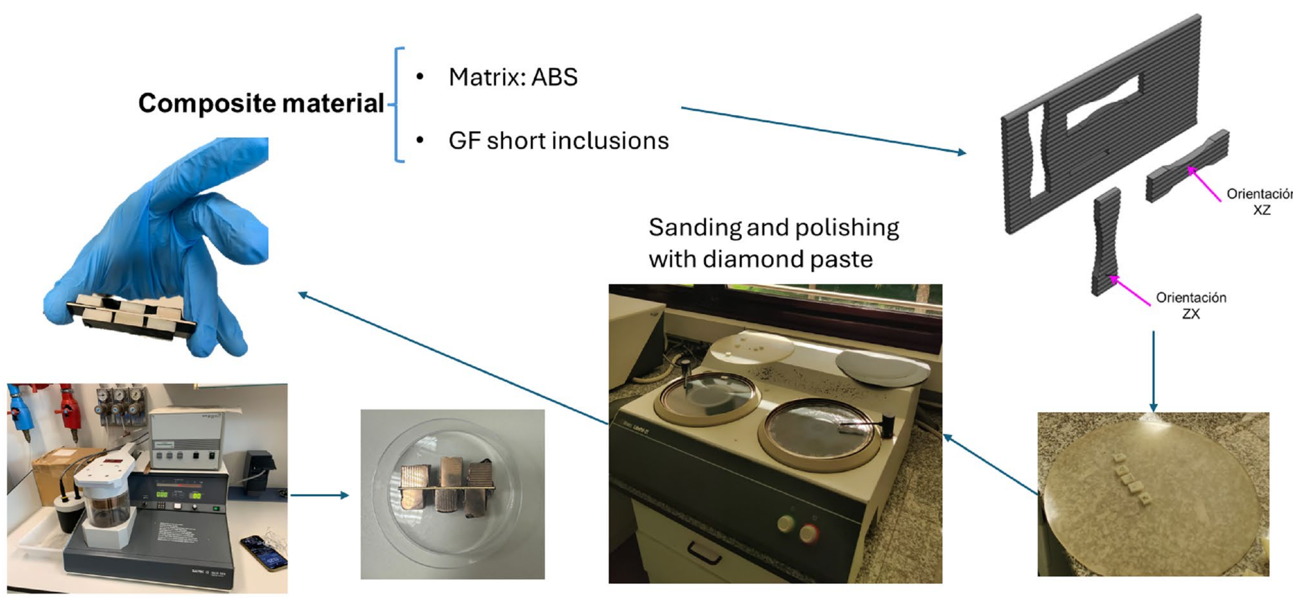

Fig. 5 Preparation of the samples to be observed under microscopy

SEM operated at a magnification of 500× to 1000× with an acceleration voltage of 5 kV, using secondary electron detection to enhance surface detail visualization. The captured images provided a 500 µm × 500 µm field of view which allowed detailed examination of fiber distribution within the polymer matrix.

2.3 Digital Image Processing for Fiber Analysis

The first step in the workflow was to transform the original image to grayscale, which improved the contrast and facilitated the segmentation process. The image processing sequence involved binarization through threshold filter application that produced a binary mask representing glass fibers as white sections against a black polymer matrix background.

The image processing sequence involved binarization through threshold filter application that produced a binary mask representing glass fibers as white sections against a black polymer matrix background. Precisely adjusting the thresholding procedure effectively reduces image noise and ensures accurate fiber segmentation. In this study, binarization was performed using a Python-based routine with a fixed grayscale cut-off value of 128 (8-bit scale). Additionally, a morphological smoothing filter was applied to reduce pore-related artifacts and improve segmentation accuracy. This step is critical, as the segmentation quality directly influences the reliability and accuracy of the subsequent morphological analysis. It should be noted that binarized masks cannot reproduce the grayscale SEM image with 100% fidelity, as the thresholding process inherently simplifies the information. Local differences, such as those observed in Fig. 6, are a normal consequence of segmentation and were minimized through the use of global Otsu thresholding and fixed morphological post-processing parameters, applied consistently across the dataset.

Each fiber contour was approximated by an ellipse through a custom Python routine. The binary mask was processed with `scikit-image` to identify connected components, and the pixel coordinates of each object were retrieved. An ellipse was then fitted to these coordinates by least-squares minimization using `OpenCV` (`cv2.fitEllipse`) or an equivalent routine. The fitted ellipses provided the geometrical descriptors later exported

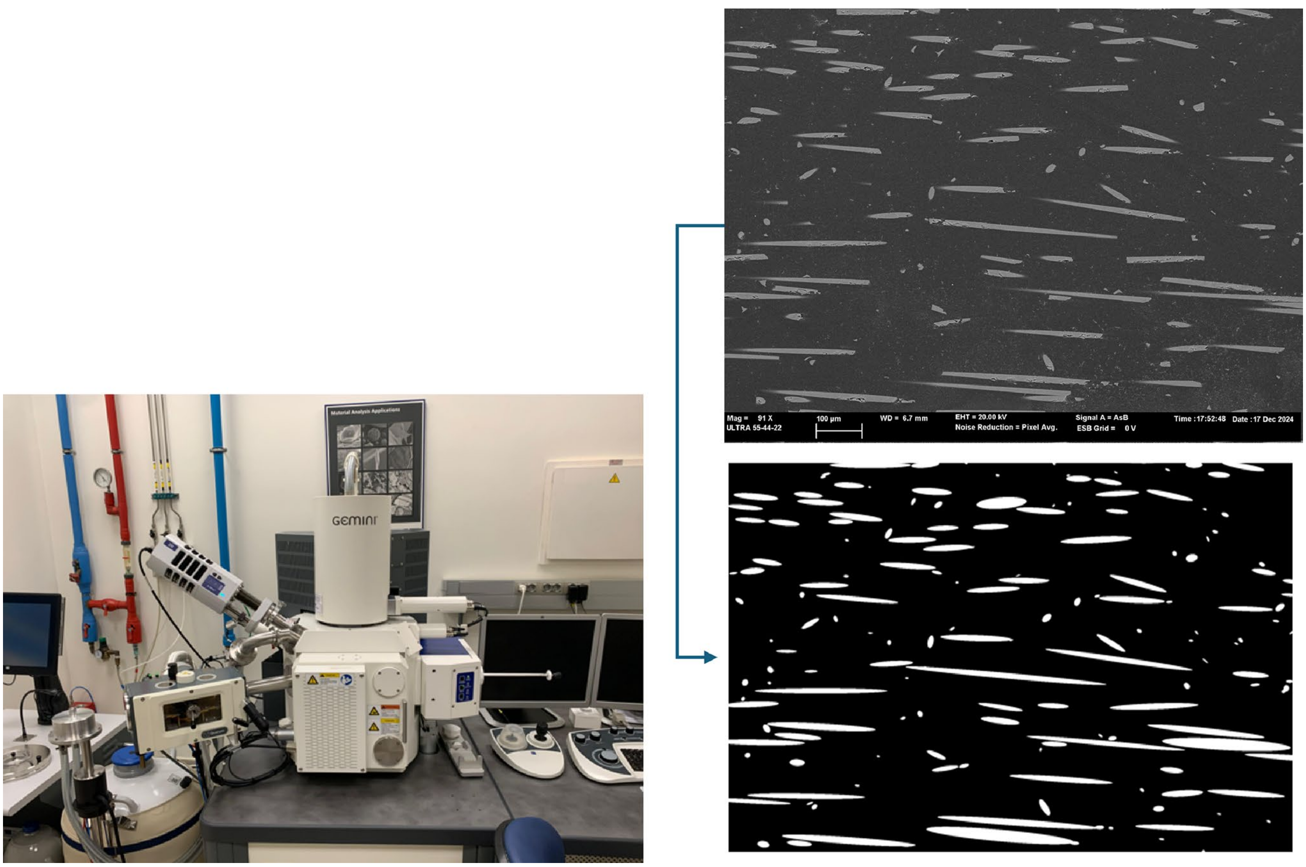

Fig. 6 Workflow for converting microscopy images into binary masks. Top row: raw FESEM image. Bottom row: binarized mask. The same region of interest (ROI) is displayed in both images for direct comparison. This figure demonstrates the preprocessing pipeline used before ellipse fitting and CNN training

as numerical arrays for subsequent tensorial analysis, as defined in Eq. (3). From these ellipses, the geometrical parameters were extracted and interpreted: the major diameter (M) as a measure of the projected fiber length, the minor diameter (m) as the projected width, and the in-plane angle (ϕ) as the orientation relative to a reference axis. Together, these descriptors capture the alignment state of the fibers and constitute the input for evaluating the anisotropy of the composite structure.

The imaging process captures a two-dimensional view of the three-dimensional fiber network, which is used to estimate the true three-dimensional orientation of each fiber. The ratio of the major-to-minor axes of the fitted ellipses (M/m) was used as a metric to estimate the fiber tilt in the out-of-plane direction. Geometric assumptions about fiber distribution allowed researchers to achieve better understanding of fiber alignment patterns through this estimation method. The second-order orientation tensor A_{ij} was used to calculate the statistical orientation of the fibers. The tensor is a critical tool for evaluating the anisotropic properties of composites and allows predictions to be made about their mechanical behavior. Advani and Tucker's formulation [7] determined the tensor components as

$$A_{xx} = \frac{1}{N}\sum_{i=1}^{N}\sin^2\beta_i, \quad A_{yy} = \frac{1}{N}\sum_{i=1}^{N}\cos^2\beta_i\sin^2\phi_i, \quad A_{zz} = \frac{1}{N}\sum_{i=1}^{N}\cos^2\beta_i\cos^2\phi_i, \tag{3}$$

where N represents the total number of fibers analyzed, β_i denotes the inclination angle of the ith fiber with respect to the out-of-plane direction, and ϕ_i corresponds to the in-plane orientation angle obtained from the ellipse fitting. The computed orientation tensor components provide a quantitative measure of fiber alignment within the composite, which is essential for understanding its mechanical behavior and optimizing processing conditions to achieve the desired material properties.

2.4 Synthetic Data Generation for Neural Network Training

Training a neural network requires large amounts of data. Thousands of images must be collected and each one must be accurately associated with its orientation tensor. There are major challenges in preparing such a dataset, as thousands of images require manual orientation tensor assessments, which take a lot of time and effort [12]. Therefore, this task was accomplished by developing a synthetic image database using a Python-based program designed to simulate realistic SEM images. The resulting database consists of synthetic images containing fibers randomly distributed throughout each image. The method assigns an orientation tensor to each image, which serves as the ground truth for training the model.

Once the dataset was finalized, it consisted of 40,000 synthetic SEM-like images generated through the proposed pipeline; each annotated with ground-truth orientation tensors. The images had a resolution of 512×384 pixels in grayscale, with fibers represented in white over a black background. To capture both isotropic and anisotropic fiber distributions, orientation angles were sampled from a Fisher distribution with concentration parameter κ. A value of $\kappa = 0$ corresponds to isotropy, while increasing κ introduces anisotropy along the target direction. The dataset was generated with a uniform coverage of κ values across the specified range, resulting in an approximately balanced proportion of isotropic and anisotropic samples. Of the complete dataset, 80% were allocated for training, while the remaining 20% were reserved for validation and testing. After training, the model was contrasted with traditional measurements and qualitatively confirmed to function correctly. The image allocation technique enables a robust evaluation of the model's accuracy in predicting fiber orientations [12, 16–18].

Production of datasets containing both isotropic and anisotropic fiber distributions during the image synthesis process depended on establishing a probability density function for fiber orientations. Fibers were represented as elongated ellipses or cylindrical cross-sections on a high-resolution binary grid during synthetic image production depending on how the slice plane was oriented. A constant contrast level between fibers and matrix was maintained to replicate SEM imaging parameters, ensuring effective neural network generalization on experimental datasets. The orientation tensor A_{ij} was computed using the second-order orientation tensor formulation which evaluated how fibers were distributed in space. The orientation tensor mathematically describes the fiber alignment patterns and highlights the principal directional characteristics within fiber assemblies. Figure 7 illustrates samples of the virtual image acquisition methodology used for training the AI model, presenting six examples corresponding to distinct fiber orientation tensors.

The algorithm employs the variables a, b, p, and Φ, where a represents the diameter of an individual glass fiber, b corresponds to the length of the major axis of the ellipse, p denotes the percentage of the total area occupied by ellipses, and Φ indicates the fiber orientation angle with respect to the z- and y-axes.

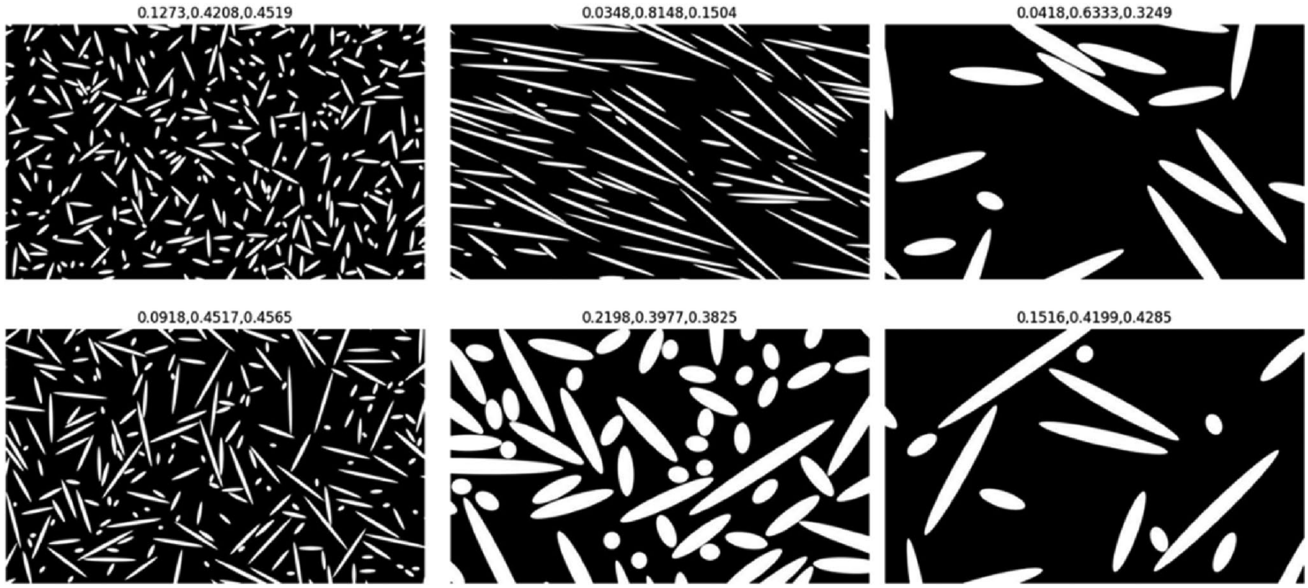

Fig. 7 Examples of synthetic SEM-like micrographs generated through the proposed pipeline. Fibers are represented in white over a black background, with varying orientation distributions that illustrate isotropic and anisotropic cases. The numerical values above each image correspond to the computed components of the second-order orientation tensor (A_{xx}, A_{yy}, A_{zz}) associated with the depicted distribution

2.5 Neural Network Implementation for Image Analysis

A tailored CNN was developed to convert microstructural image data into quantitative orientation tensor components. It directly predicts the fiber orientation tensor components (A_{xx}, A_{yy}, A_{zz}) from binarized SEM-like images. Unlike classical approaches that depend on detecting and fitting each ellipse individually, the proposed CNN consumes the entire binarized micrograph and directly regresses the orientation tensor. This strategy reduces sensitivity to segmentation artifacts, partial fibers, polishing defects, and overlapping features that can bias ellipse-based measurements. Moreover, once trained, the CNN performs inference in near real time, enabling the analysis of large datasets without the computational cost of per-object fitting. While the ellipse-fitting method provides good estimates when objects are clearly identifiable, the CNN offers higher robustness, scalability, and automation.

The final CNN architecture consisted of three convolutional blocks followed by two fully connected layers. The first convolutional block used 16 filters (kernel size = 3, stride = 1, padding = 1) with ReLU activation and a 2×2 max pooling layer. The second block used 32 filters with the same kernel and pooling configuration, and the third block used 64 filters followed by adaptive average pooling to 4×4. The flattened output (1024 features) was passed to a fully connected layer of 256 units with ReLU activation and dropout ($p = 0.10$), and finally to a linear output layer of 3 units corresponding to the tensor components (A_{xx}, A_{yy}, A_{zz}). Training used the Adam optimizer (learning rate = 0.001), mean squared error loss, batch size = 16, and 150 epochs [19, 20].

The resulting feature maps are flattened and passed to fully connected Multi-Layer Perceptrons (MLPs), which produce the final predictions. To improve generalization and prevent overfitting, a dropout layer randomly disables 10% of the neurons during training. As the goal here is to predict continuous values of the orientation tensor rather than class labels, a linear activation is used in the output layer instead of the commonly used SoftMax in classification tasks. This choice enables the network to predict continuous tensor values directly, which is essential for precise fiber orientation estimation. Figure 8 illustrates the architecture layout, highlighting the key layers responsible for feature extraction, dimensionality reduction, and final regression output. Training was performed using Adam optimization (learning rate = 0.001) and Mean Squared Error (MSE) loss function to ensure accurate predictions [15].

CNNs initially extract image features through convolutional layers, followed by the application of nonlinear activation functions (such as Rectified Linear Units, ReLU) and pooling layers. However, training deep networks can become increasingly challenging due to shifts in activation distributions across layers, a phenomenon known as *internal covariate shift*. Batch Normalization addresses this issue by standardizing the activations within each mini-batch before passing them to subsequent layers, resulting in stabilized

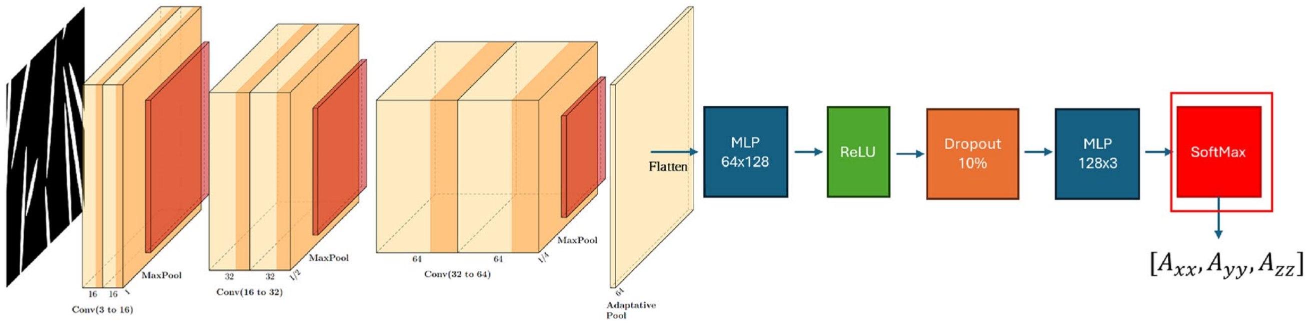

Fig. 8 Convolutional neural network architecture for fiber orientation tensor prediction

training, reduced sensitivity to initializations, and improved convergence speed. The Batch Normalization should be performed as

$$\hat{x}_i = \frac{x_i - \mu_B}{\sqrt{\sigma_B^2 + \epsilon}}, \tag{4}$$

where x_i is the input activation before normalization; μ_B is the mean of activations within the current batch

$$\mu_B = \frac{1}{m} \sum_{i=1}^{m} x_i, \tag{5}$$

being m the number of examples in the batch. Finally, σ_B^2 is the variance within the batch

$$\sigma_B^2 = \frac{1}{m} \sum_{i=1}^{m} (x_i - \mu_B)^2, \tag{6}$$

and ϵ is a small constant (typically 10^{-5}) added for numerical stability to avoid division by zero.

After normalization, a learnable affine transformation is applied, introducing scale and shift parameters to restore the network's representational capacity

$$y_i = \gamma \hat{x}_i + \beta, \tag{7}$$

where γ and β are hyperparameters that enable the network to dynamically scale and shift the normalized activations, thus restoring flexibility and improving representational capacity.

This transformation helps Batch Normalization stabilize training while preserving the network's ability to learn complex patterns. Adaptive pooling produces feature maps with fixed output dimensions regardless of varying input sizes as illustrated in Fig. 7. Max and average pooling operations use unchanging kernel sizes and strides while adaptive pooling adjusts pooling regions dynamically to keep a specific output shape. The first convolutional layers extract hierarchical features from the input image while expanding the channel count and reducing spatial dimensions. Max pooling functions to shrink the dimensions of intermediate feature maps which reduces computational demand while preserving important features. The integration of an adaptive pooling layer before flattening ensures standardized feature map dimensions for input images of various sizes before they move to fully connected layers. Flattening changes the fixed-size feature map into one-dimensional vector space [21]. In this case, adaptive pooling produces a feature map that, when flattened, results in a 64-dimensional output

$$\text{Flattened Output} = H_{\text{out}} \times W_{\text{out}} = 64, \tag{8}$$

where H_{out} and W_{out} represent the height and width of the desired output dimensions.

This architectural design ensures both robustness and accuracy when extracting orientation features from SEM images. By combining convolutional layers, adaptive pooling, and regularization techniques such as dropout, the network achieves reliable generalization, which is essential for characterizing complex fiber distributions in additive manufacturing composites [22].

3 Results and Discussion

3.1 Convolutional Neural Network Architecture

To evaluate the effectiveness of the proposed neural network, a comprehensive analysis of its training and validation performance was conducted. The network was trained on a dataset of synthetic microscopy images generated to simulate a wide range of fiber orientation patterns. The dataset was divided into three distinct subsets: 80% was used for training, and the remaining 20% was evenly split between validation and testing (10% each). This strategy aimed to enhance the model's learning capability while reserving sufficient unseen data to support robust evaluation. Training was conducted over 150 epochs, using the Adam optimizer, which was selected due to its ability to handle sparse gradients and dynamically adjust learning rates. An initial learning rate of 0.001 was applied, and adaptive moment estimation combined with momentum-based updates contributed to improved convergence stability and computational efficiency (see Table 2).

A batch size of 16 was chosen to balance memory consumption with gradient stability. The Mean Squared Error (MSE) loss function was used to measure the discrepancy between predicted and actual values of the fiber orientation tensor components, ensuring accurate regression-based predictions [23, 24].

The training process employed an adaptive learning rate scheduler, which dynamically adjusted learning rates based on validation loss trends. This strategy effectively prevented stagnation during training and reduced the risks of both overfitting and underfitting by continuously optimizing weight updates. Leveraging the computational efficiency provided by a high-performance GPU, the total training time was reduced to approximately 4 h. Figure 9 presents a quantitative evaluation of CNN prediction accuracy through a comparison between actual tensor component A_{xx} values and the predicted model outputs. The scatter plot shows dense data point clustering along its diagonal which reveals a strong connection between predicted model values and actual measurements. The model shows successful acquisition of statistical fiber orientation distribution for composite materials based on its diagonal pattern alignment. Small discrepancies between predicted tensor values and actual tensor values occur at higher tensor values which result in minor over- or under-estimation. High tensor values produce data representation challenges and fiber orientation variability in certain microstructures generates complexity which leads to deviations. The primary pattern matches the anticipated correlation which demonstrates that the CNN produces accurate predictions for fiber orientation tensors [25].

Table 2 Training configuration parameters

Configuration	Value
Training set size	80%
Validation set size	10%
Test set size	10%
Learning rate	0.001
Epochs	150
Batch size	16
Loss function	Mean squared error (MSE)
Optimizer	Adam
Learning rate scheduler	Enabled
Training time	4 h

Tensor components scatter plots for A_{yy} and A_{zz} provide supplementary evidence to demonstrate the model's predictive power beyond the A_{xx} component. The scatter plots demonstrate a near-perfect correlation with coefficients approaching 1.00, which confirms that the CNN model captures fiber orientation features effectively across all tensor components. The tight clustering of data points along the diagonal indicates that the model retains generalization capabilities beyond its training set, reducing the risk of overfitting and ensuring reliable predictions for new data. The CNN effectively captures the anisotropic properties of fiber orientation in composites, as evidenced by its consistent prediction accuracy across all three tensor components.

Figure 9 provides substantial evidence that the CNN delivers high precision results in fiber orientation tensor predictions. Optimized hyperparameters and an adaptive learning rate scheduler combined with a structured training-validation framework resulted in a model that effectively detects complex microstructural patterns. The analysis performed by CNN-based models proves effective for fiber-reinforced composites and promotes advancements in automated material characterization and design optimization.

Figure 10 illustrates the variations of training loss, validation loss, and test loss throughout multiple epochs based on the learning curve. The horizontal axis indicates epoch counts, while the vertical axis measures loss values using a logarithmic scale. The early phase of training shows high starting points for all three loss curves but the training (red) and test loss (green) decrease in a more consistent manner than the validation loss (blue) which exhibits irregular patterns. The model effectively learns from the data as the training loss demonstrates a steady decline over time. The validation loss decreases over time but displays larger fluctuations which indicate inconsistent performance on new data. The parallel downward trends observed in validation and test losses suggest that the model generalizes effectively; however, minor overfitting is indicated by the training loss consistently remaining lower than both validation and test losses. The consistent reduction across all curves shows effective training yet fluctuations in validation and test losses indicate potential improvements for model stability through regularization techniques. It is observed that the training loss remains slightly higher than the validation and test losses. This behavior is explained by the use of dropout ($p = 0.10$), which is active only during training and artificially increases the apparent loss. During validation and testing, dropout is disabled, leading to lower measured errors. This difference therefore reflects the regularization strategy rather than overfitting.

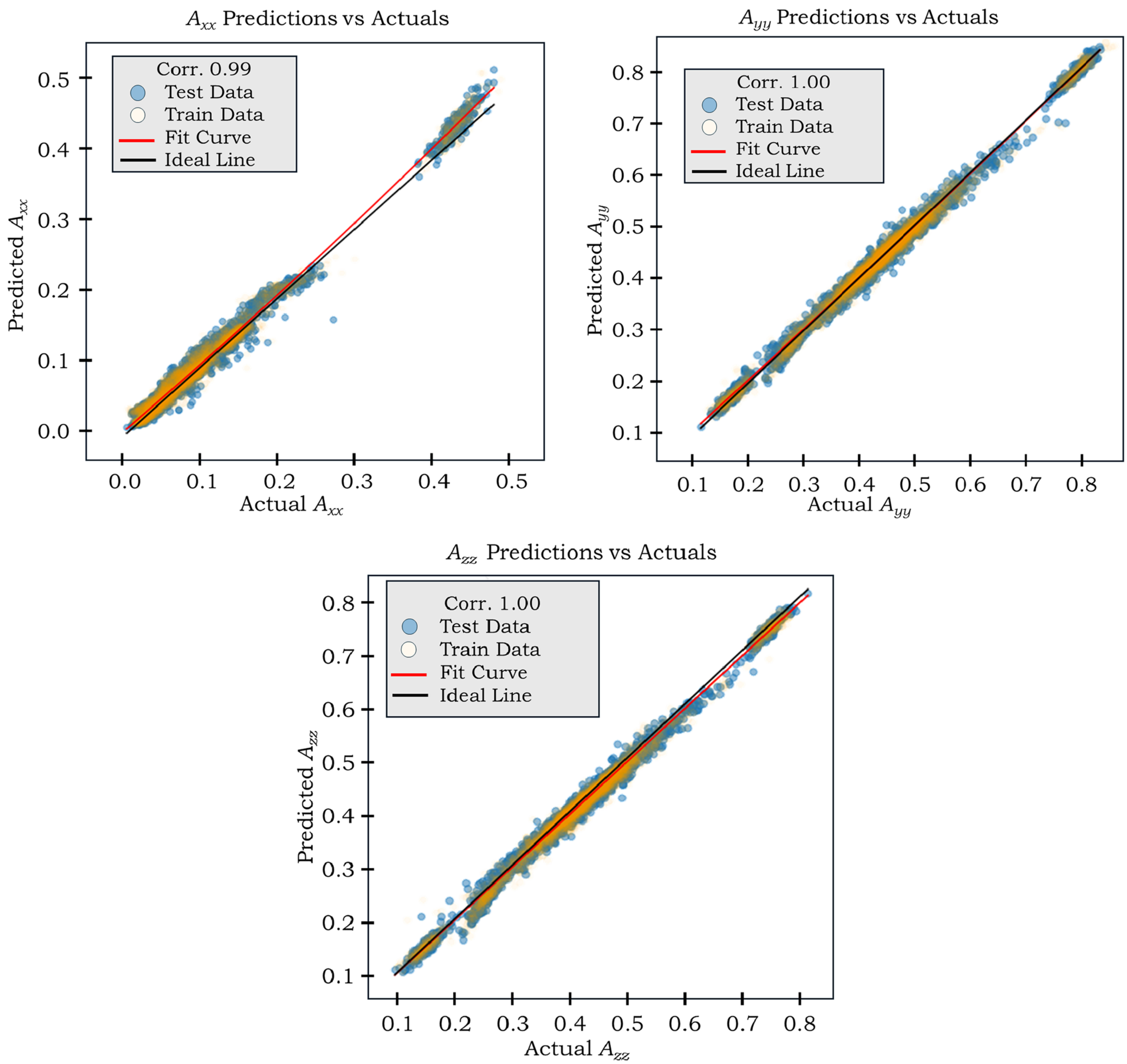

Fig. 9 Deep learning: training and results

3.2 Model Validation

Accurate evaluation of the performance of machine learning model performance requires testing on data that remain completely separate from the training data set. The evaluation method uses a 20% sample of images that were not available during training to test the model. By evaluating the model's performance on new sets of data, the validation process allows us to determine whether the model is learning accurate predictions rather than patterns. The validation process is a crucial technique for identifying instances of overfitting, since it enables the assessment of a model's ability to maintain its performance on unseen data following training on a limited set of known data. The images in Fig. 11 show four synthetic microstructure patterns, the real tensor, the predicted tensor, and then the mean angle error.

Tables 3 and 4 present the model performance metrics throughout the training, validation, and testing phases for multiple datasets. The Mean Angular Error represents the average angular deviation (in degrees) between the predicted and the reference vectors. In this context, it quantifies how accurately the model predicts the orientation or direction of the tensor components. A lower Mean Angular Error indicates a smaller difference between predicted and true

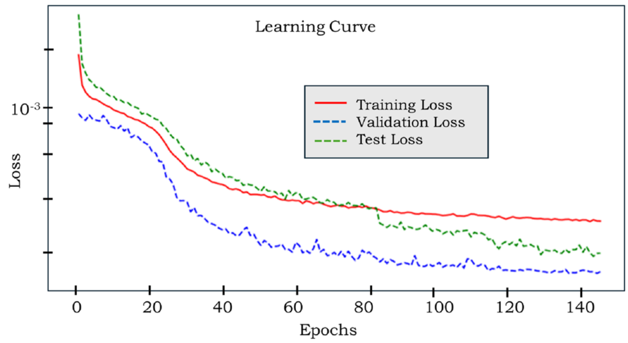

Fig. 10 Learning curves (MSE loss) for training, validation, and test sets across epochs. The higher training loss is due to dropout being active during training only, whereas it is disabled during validation and testing (see Sect. 3.1). This figure illustrates stable convergence and generalization of the model

orientations, meaning a more precise estimation of the vector field or tensor directions. The model evaluation consists of mean angular error measurements along with similarity and Pearson correlation coefficients determined for each dataset partition. The model demonstrates high precision in estimating fiber orientations, because it maintains cosine similarity values above 0.999 and angular errors between 1.3° and 1.4°. Global error metrics indicate strong alignment between true values and predicted outcomes due to a R^2 value of 0.98937 that shows minimal deviation. The model shows minimal performance degradation when predicting fiber orientation in training, validation, and test data sets.

Figure 12 shows the *k*-fold cross-validation method and a summary table of evaluation metrics obtained across five different folds is presented in Table 5. The mean row corresponds to the average performance of the model computed across the five cross-validation folds. Each metric is averaged to provide a global indicator of model accuracy and stability. This allows assessing how consistently the model

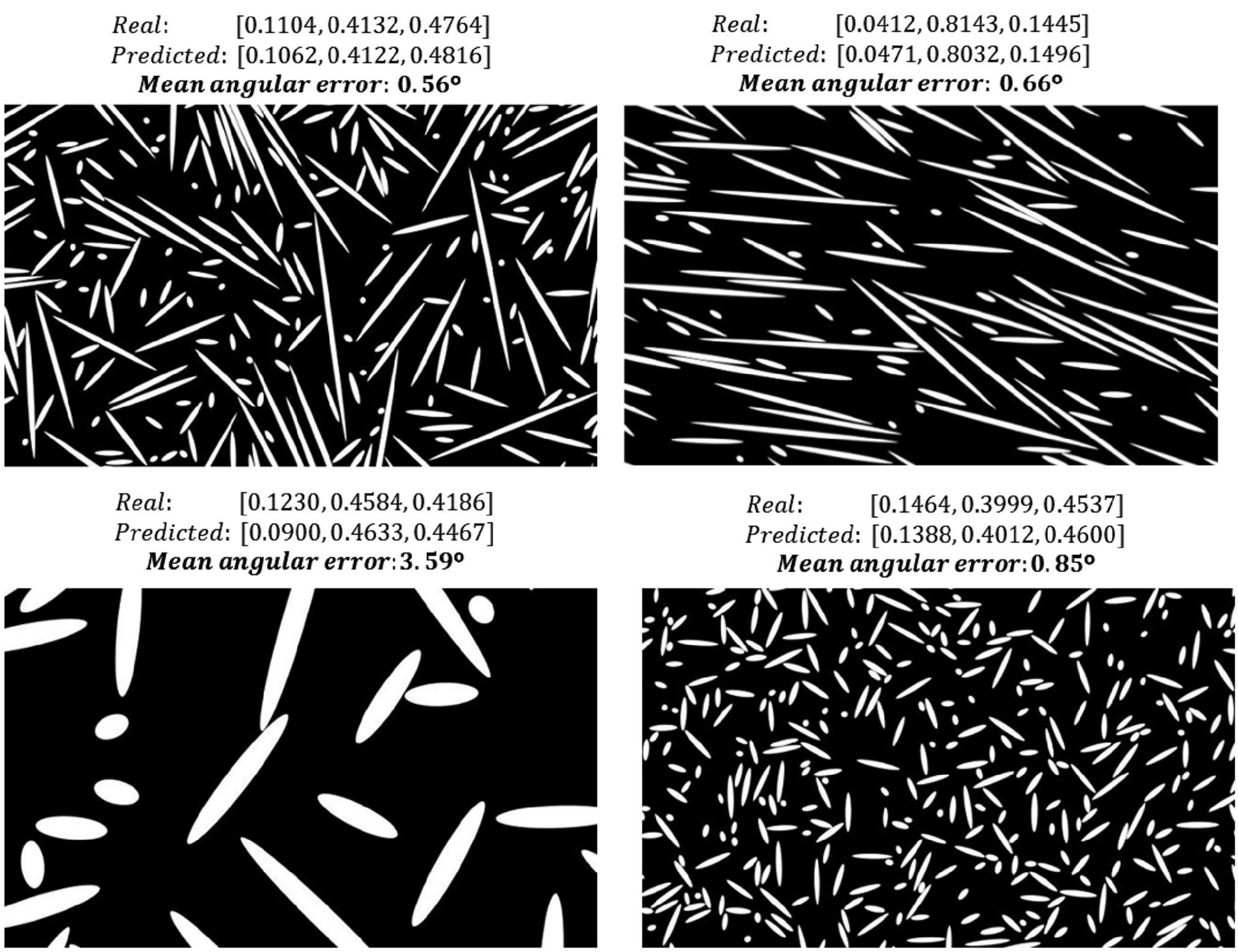

Fig. 11 Images tested for model validation

Table 3 Performance metrics for training, validation, and test datasets

Dataset	Metric	Value
Training	Mean Cosine Similarity	0.99953
	Mean Angular Error [°]	**1.39502**
	Pearson Correlation (A_{xx})	0.99356
Validation	Mean Cosine Similarity	0.99951
	Mean Angular Error [°]	**1.42294**
	Pearson Correlation (A_{yy})	0.99359
Test	Mean Cosine Similarity	0.99962
	Mean Angular Error [°]	**1.26876**
	Pearson Correlation (A_{zz})	0.99453

Table 4 Global performance metrics

Metric	Value
Jensen–Shannon Divergence (JSD)	0.00023
Mean Absolute Error (MAE)	0.00809
Mean Absolute Percentage Error (MAPE) [%]	4.78343
Mean Squared Error (MSE)	0.00012
Coefficient of Determination (R^2)	0.98937
Root Mean Squared Error (RMSE)	0.01108

performs across different subsets of the data, reducing bias from any single fold. The diagram depicts the division of the data set into five separate subsets where each fold operates as a test set, while the rest of the data serve as the training set. The evaluation method achieves robustness by averaging results from multiple data partitions. Table 5 presents both mean values and standard deviations (σ) for each performance metric during the k-fold cross-validation process, which includes JSD, MAE, MAPE, MSE, R^2, and RMSE, and demonstrates a minimal prediction error through MAE of 0.008046, MSE of 0.000144, and RMSE of 0.011073. The very low MAE of 0.008046 along with an MSE of 0.000144 and an RMSE of 0.011073 means that the model has minimal prediction error. The model demonstrates high accuracy through its R^2 score of 0.989116 which shows that the predicted outputs match the actual data well.

Across all training splits, the model maintains uniform performance, evidenced by low standard deviations across all performance metrics. The evaluation results indicate that data segment variance remains minimal while model operation exhibits both efficiency and stability. Cross-validation eliminates data split bias, which in turn ensures consistent performance metrics helping users trust the model's reliability.

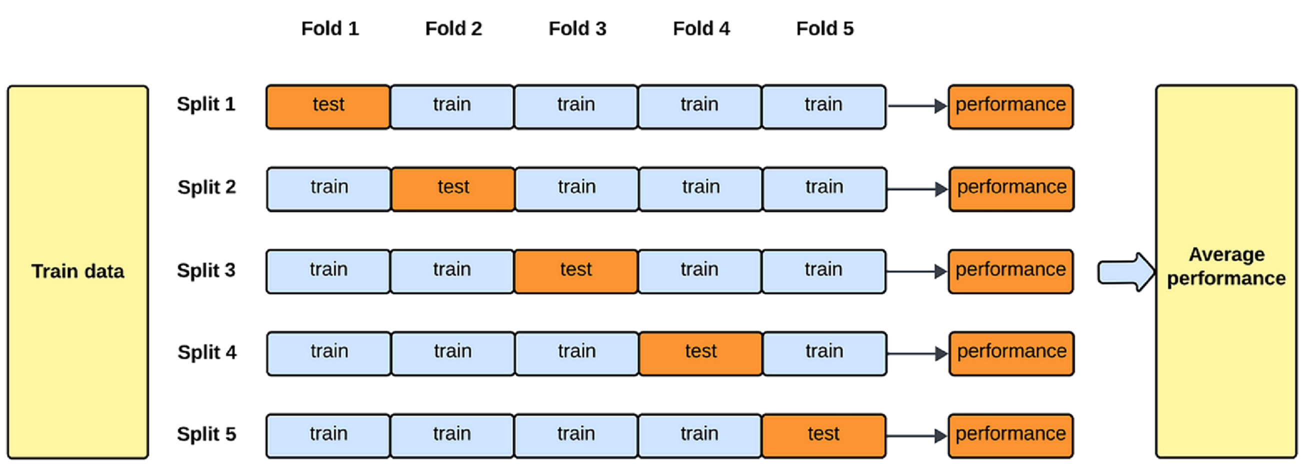

Fig. 12 *K*-fold cross-validation scheme

Table 5 Global performance metrics across five cross-validation folds, including mean values and standard deviation (σ) for each metric

Fold	JSD	MAE	MAPE [%]	MSE	R^2	RMSE
Fold 1	0.000217	0.007402	4.782471	0.000183	0.989594	0.011109
Fold 2	0.000275	0.007206	4.784370	0.000100	0.988649	0.011050
Fold 3	0.000253	0.008822	4.784095	0.000122	0.988954	0.011081
Fold 4	0.000240	0.008292	4.782855	0.000113	0.989103	0.011089
Fold 5	0.000196	0.008506	4.782794	0.000199	0.989282	0.011035
Mean	**0.000236**	**0.008046**	**4.783317**	**0.000144**	**0.989116**	**0.011073**
σ	0.000030	0.000710	0.000850	0.000040	0.000350	0.000030

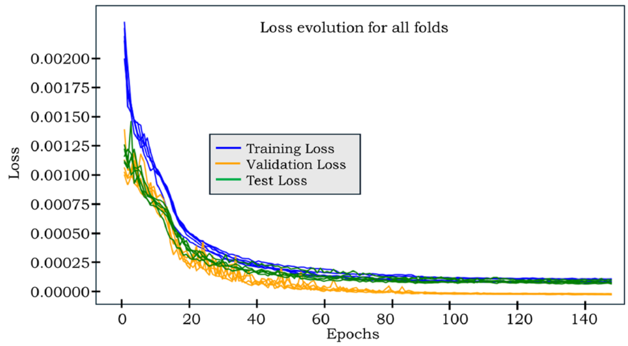

Fig. 13 Loss evolution across all folds

Figure 13 presents the loss evolution across all folds during testing, training, and validation phases. Epoch numbers appear on the x-axis, while loss values appear on the y-axis in the plot. The initially high training loss (blue) experiences a steep decline during the first 20 epochs before decreasing gradually to reach a stable state. Validation (orange) and test (green) loss patterns show that the model maintains strong generalization capabilities while avoiding noticeable overfitting. Every learning phase shows effective performance when the loss curves reach their lowest point and stabilize after approximately 100 epochs.

The measurement method for orientation tensors is illustrated using an LFAM example in Fig. 14. This study compares deep learning techniques and manual methods to determine fiber orientations. The graph shows an example image with red outlines to highlight the fibers on the left side. The fiber alignment in the LFAM printed sample gets demonstrated through the orientation tensor values (A_{xx} = 0.11533, A_{yy} = 0.78703, A_{zz} = 0.09764). The researchers generated the weighted average tensor $\bar{T}$ through the combination of multiple zoomed images from the specified image. The calculation weight of each image diminishes when zoom levels rise to maintain balance in the final tensor calculation. The traditional manual approach leads to inconsistent results, since it requires a lengthy process and users interpret it differently. Tensor estimation becomes automated through a deep learning-based approach that processes labeled data using a trained neural network. The method ensures precise fiber orientation extraction through its efficient processing which guarantees analytical precision with reliable results. Due to its powerful generalization capabilities for new samples, the model generates reliable fiber orientation characterization results.

4 Conclusions

This study presents a deep learning-based methodology for characterizing fiber orientation in composite materials produced via Material Extrusion Large Format Additive Manufacturing (MEX-LFAM). By combining synthetic image generation with CNNs, we developed a scalable approach that eliminates the reliance on time-consuming microscopy-based analyses while maintaining high predictive accuracy. The results demonstrate that CNN models trained on synthetic datasets can accurately predict fiber orientation tensors from real microscopy images, achieving a strong correlation with experimental data. This confirms the feasibility and efficiency of using AI-driven techniques for fiber orientation assessment in composite manufacturing.

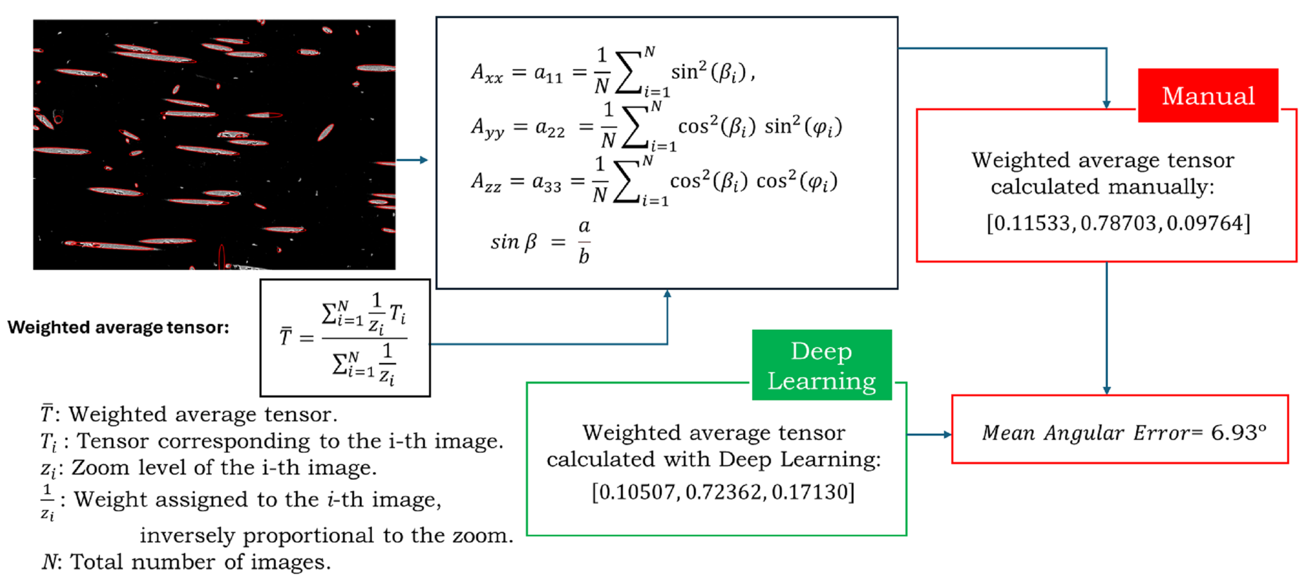

Fig. 14 Comparison between manual (red fiber measurement) and deep learning-based estimation of the weighted average orientation tensor

The present work establishes a validated and reproducible methodology that combines synthetic image generation, a CNN regressor, and a standardized preprocessing workflow. These contributions are deployable as they stand and provide immediate value for automated fiber orientation analysis in LFAM and related processes. Future directions, such as physics-informed neural networks and X-ray microtomography, are highlighted only as potential extensions beyond the scope of the present study.

While the proposed method significantly reduces computational and experimental overhead, further improvements can be made. Future work will focus on enhancing dataset generation by incorporating physics-informed neural networks (PINNs) to improve model generalization and interpretability. Additionally, integrating high-resolution imaging techniques such as X-ray microtomography could provide more robust validation and refine fiber orientation predictions.

Overall, this study highlights the potential of deep learning to revolutionize fiber-reinforced polymer characterization, paving the way for more efficient process optimization, material design, and quality control in additive manufacturing.

Acknowledgements This research received partial funding from the Government of Spain under Project No. PID2023-151110OB-I00 and Generalitat Valenciana under CIPROM/2022/3 and CIACIF/2021/286. This research project is part of the program DesCartes and is supported by the National Research Foundation, Prime Minister's Office, Singapore under its Campus for Research Excellence and Technological Enterprise (CREATE) program.

Data Availability The data from this work are available upon request from the authors.

Declarations

Conflict of interest The authors declare no conflict of interest.

References

1. Z. Zhang, K. Song, Y. Pan, J. He, S. Umezu, Spatial mechanical enhancement strategy enabled by multi-axis material extrusion additive manufacturing. J. Manuf. Process. **134**(1), 762–774 (2025). https://doi.org/10.1016/j.jmapro.2025.01.002
2. P. Yeole, S. Kim, A. Arabi Hassen, V. Kumar, V. Kunc, U. Vaidya, Large-scale additive manufacturing tooling for extrusion-compression molds. Addit. Manuf. Lett. **1**(1), 100007 (2021). https://doi.org/10.1016/j.addlet.2021.100007
3. P. Bleiziffer, J. Hofmann, R. Zboray, T. Wiege, R. Herger, Predicting the fiber orientation in glass fiber reinforced polymers using the moment of inertia and convolutional neural networks. Eng. Appl. Artif. Intell. **104**(1), 104351 (2021). https://doi.org/10.1016/j.engappai.2021.104351
4. D. Shen, Z. Wu, A method for measuring the orientation of carbon fiber weave. Fibers Polym. **22**(12), 3501–3509 (2021). https://doi.org/10.1007/s12221-021-0912-2
5. A. Pathak, H. Garg, K. Subhedar, S. Dhakate, Significance of carbon fiber orientation on thermomechanical properties of carbon fiber reinforced epoxy composite. Fibers Polym. **22**(7), 1923–1933 (2021). https://doi.org/10.1007/s12221-021-0703-9
6. N. Kalimullah, S. Ojha, M. Radzieński, A. Shelke, A. Habib, A probabilistic machine learning framework for stiffness tensor estimation of carbon composite laminate. Mech. Syst. Signal Process. **223**(1), 111872 (2025). https://doi.org/10.1016/j.ymssp.2024.111872
7. S.G. Advani, C.L. Tucker, The use of tensors to describe and predict fiber orientation in short fiber composites. J. Rheol. **31**(8), 751–784 (1987). https://doi.org/10.1122/1.549945
8. B. Šeta, M. Sandberg, M. Brander, M.T. Mollah, D. Pokkalla, V. Kumar, J. Spangenberg, Modeling fiber orientation and strand shape morphology in three-dimensional material extrusion additive manufacturing. Compos. B Eng. **266**(1), 110957 (2023). https://doi.org/10.1016/j.compositesb.2023.110957
9. C.L. Tucker III., *Fundamentals of Fiber Orientation: Description, Measurement and Prediction* (Hanser, Munich, 2022)
10. Y. Li, W. Ge, B. Liu, Z. Wang, C. Wang, Y. Zhang, Collaborative optimization of composite structure and fiber orientation through real-time correction of deep neural network (DNN) models with elite samples. Mech. Adv. Mater. Struct. **31**(26), 7944–7956 (2024). https://doi.org/10.1080/15376494.2023.2253018
11. T. Herrmann, D. Niedziela, D. Salimova, T. Schweiger, Predicting the fiber orientation of injection molded components and the geometry influence with neural networks. J. Compos. Mater. **58**(15), 1801–1811 (2024). https://doi.org/10.1177/00219983241248216
12. A. Bauer, S. Trapp, M. Stenger, R. Leppich, S. Kounev, M. Leznik, K. Chard, I. Foster, Comprehensive exploration of synthetic data generation: a survey (2024), Preprint at arXiv: 2401.02524
13. J. Li, H. Ye, Y. Dong, Z. Liu, T. Sun, H. Wu, An efficient deep learning-based topology optimization method for continuous fiber composite structure. Acta Mech. Sin. **41**(4), 424207 (2025). https://doi.org/10.1007/s10409-024-24207-x
14. Y. Wang, S. Xu, K. Bwar, B. Eisenbart, G. Lu, A. Belaadi, B. Fox, B. Chai, Application of machine learning for composite moulding process modelling. Compos. Commun. **48**(1), 101960 (2024). https://doi.org/10.1016/j.coco.2024.101960
15. M. Agarwal, P. Pasupathy, X. Wu, S.S. Recchia, A.A. Pelegri, Multiscale computational and artificial intelligence models of linear and nonlinear composites: a review. Small Sci. (2024). https://doi.org/10.1002/smsc.202300185

16. M.M. Azad, S. Kim, H.S. Kim, Autonomous data-driven delamination detection in laminated composites with limited and imbalanced data. Alex. Eng. J. **107**(1), 770–785 (2024). https://doi.org/10.1016/j.aej.2024.09.004
17. S. McKnight, S. Pierce, E. Mohseni, C. MacKinnon, C. MacLeod, T. O'Hare, C. Loukas, A comparison of methods for generating synthetic training data for domain adaption of deep learning models in ultrasonic non-destructive evaluation. NDT & E Int. **141**(1), 102978 (2024). https://doi.org/10.1016/j.ndteint.2023.102978
18. R. Guo, M. Alves, M. Mehdikhani, C. Breite, Y. Swolfs, Synthesising realistic 2D microstructures of unidirectional fibre-reinforced composites with a generative adversarial network. Compos. Sci. Technol. **250**(1), 110539 (2024). https://doi.org/10.1016/j.compscitech.2024.110539
19. J. Barman, C. Kuo, Fully automatic and precisely woven fabric defect detection using improved yolov7-tiny model utilizing enhanced residual convolutional network. Fibers Polym. **26**(1), 353–368 (2025). https://doi.org/10.1007/s12221-024-00811-1
20. Z. Xiao, L. Pei, L. Geng, Y. Sun, F. Zhang, J. Wu, Surface parameter measurement of braided composite preform based on faster R-CNN. Fibers Polym. **21**(3), 590–603 (2020). https://doi.org/10.1007/s12221-020-9425-7
21. V. Daghigh, S.B. Ramezani, H. Daghigh, T.E. Lacy, Explainable artificial intelligence prediction of defect characterization in composite materials. Compos. Sci. Technol. **256**(1), 110759 (2024). https://doi.org/10.1016/j.compscitech.2024.110759
22. M. Hamza, L. Borkowski, A. Chattopadhyay, Physics-Informed Machine Learning Model for Ceramic Matrix Composite Creep (2025). https://doi.org/10.2514/6.2025-2516
23. C. Tang, J. Zou, Y. Xiong, B. Liang, W. Zhang, Automatic reconstruction of closely packed fabric composite RVEs using yarn-level micro-CT images processed by convolutional neural networks (CNNS) and based on physical characteristics. Compos. Sci. Technol. **252**(1), 110616 (2024). https://doi.org/10.1016/j.compscitech.2024.110616
24. C. Sanchez, E. Pineda, B. Hearley, J. Stuckner, T. Ricks, P. Gustafson, A Convolutional Neural Network for Enhancement of Multi-Scale Localization in Fiber-Reinforced Polymer Matrix Composite Representative Unit Cells (2025). https://doi.org/10.2514/6.2025-2519
25. Q. Zhou, H. Sun, P. Chen, G. Chen, S. Wang, H. Wang, Research on the defect detection algorithm of warp-knitted fabrics based on improved YOLOv5. Fibers Polym. **24**(8), 2903–2919 (2023). https://doi.org/10.1007/s12221-023-00253-1